Coalescence in semiconcentrated emulsions in simple shear flow

A. V. Korobko,[a] D. van den Ende, W. G. M. Agterof, and J. Mellema
Physics of Complex Fluids, Institute of Mechanics, Processes and Control—Twente (IMPACT) and J.M. Burgerscentrum, Department of Science and Technology, University of Twente, P.O. Box 217, 7500 AE Enschede, The Netherlands

(Received 1 June 2005; accepted 21 September 2005; published online 29 November 2005)

The coalescence frequency in emulsions containing droplets with a low viscosity (viscosity ratio ~0.005) in simple shear flow has been investigated experimentally at several volume fractions of the dispersed phase (2%–14%) and several values of the shear rate ($0.1-10\ s^{-1}$). The evolution of the size distribution was monitored to determine the average coalescence probability from the decay of the total number of droplets. Theoretically models for two-droplet coalescence are considered, where the probability is given by $P_c=\exp(-\tau_{dr}/\tau_{int})$. Since the drainage time τ_{dr} depends on the size of the two colliding droplets, and the collision time τ_{int} depends on the initial orientation of the colliding droplets, the calculated coalescence probability was averaged over the initial orientation distribution and the experimental size distribution. This averaged probability was compared to the experimentally obtained coalescence frequency. The experimental results indicate that (1) to predict the average coalescence probability one has to take into account the full size distribution of the droplets; (2) the coalescence process is best described by the "partially mobile deformable interface" model or the "fully immobile deformable interface" model of Chesters [A. K. Chesters, Chem. Eng. Res. Des. **69**, 259 (1991)]; and (3) independent of the models used it was concluded that the ratio τ_{dr}/τ_{int} scales with the coalescence radius to a power (2 ± 1) and with the rate of shear to a power (1.5 ± 1). The critical coalescence radius R_o, above which hardly any coalescence occurs is about 10 μm. © *2005 American Institute of Physics*. [DOI: 10.1063/1.2121627]

I. INTRODUCTION

Liquid-liquid dispersions (emulsions) with diverse physical properties play an important role in many practical and industrial applications, such as food processing, pharmacy, energy, and plastics engineering.[1–3] Parameters such as the viscosity and elasticity of the liquids, the type of flow and its strength, the size of the droplets, and the presence, or not, of surfactants play an important role in the development of the morphology during preparation and determine the subsequent stability of the emulsion after.

To understand the development of the morphology of emulsions, the kinetic processes of coalescence and breakup of droplets should be investigated in relation to the above-mentioned parameters. At low shear rates, when the shear stresses are small compared to the interface stresses, coalescence is the dominant process,[4] while breakup of droplets[5] occurs at high shear stresses. In the intermediate regime both coalescence and breakup are possible.[6] The concentration of the dispersed phase is another important parameter to control both the coalescence and the breakup processes. In this article we focus on the coalescence process of semiconcentrated emulsions in a simple shear flow.

For investigating the morphology development, several theoretical models have been put forward to describe the coalescence process in terms of the hydrodynamic and van der Waals interactions between the colliding droplets. Experiments have been performed to test these models.[7–17] In the most simple approach the interaction between the droplets is neglected and every collision between two droplets results in coalescence which leads to the Smoluchowski collision rate[18] and an exponential growth of the droplet size in time. This scenario is not in accordance with the experimental observations, and the coalescence rate has to be described as the product of the collision rate and the coalescence probability between two colliding droplets. The probability is governed by the development of the thin liquid film between the droplets, which is controlled by the interfaces and the mutual hydrodynamic and thermodynamic interactions.[19]

To describe the coalescence of droplets in simple shear flow, we first consider the formation of this film and its drainage. Two spherical droplets initially at large distance are driven towards each other by the shear flow. When the distance between the surfaces of the droplets becomes comparable with their diameters, the film formation begins as well as its drainage. The drainage is controlled by, on one side, the hydrodynamic forces in the film resisting the relative motion of the droplets and, on the other side, the external shear and attractive thermodynamic forces. The mobility of the interfaces and the deformability of the droplets play an important role in the drainage. Davis *et al.* showed that the velocity profile of the liquid in the film is the sum of a plug and a Poiseuille profile.[20] In case of very large viscosity ratios $\lambda=\eta_d/\eta_c$ (fully immobile interfaces) the drainage of the film is controlled by the viscosity of the continuous phase

[a]Author to whom correspondence should be addressed. Present address: Leiden Institute of Chemistry, Leiden University, P.O. Box 9502, 2300 RA Leiden, The Netherlands. Electronic mail: a.korobko@chem.leidenuniv.nl

while the droplets hardly deform and there is no motion in the interface. For moderate values of the viscosity ratio (partially mobile interfaces), both Poiseuille and plug profiles are established, and the drainage depends on the velocity in the interface. For very low viscosity ratios, $\lambda < 0.01$ (mobile interface), the drainage of the film is accompanied by a plug velocity profile controlled by the viscosity of the continuous phase.[21]

Below a certain film thickness the attractive van der Waals forces dominate the drainage rate of the film, resulting in a sudden decrease of the film thickness. Eventually the thermal fluctuations in the film become sufficient to rupture it.

The dynamics of the liquid film between colliding deformable droplets was studied intensively in the limits of a constant interaction force,[22–24] or a constant relative velocity of the droplets.[21,24] These two limits are idealizations of the real coalescence process,[7,25] where both the interaction force and the velocity are time dependent and determined by the motion of the droplets during the collision. At the later stage of the drainage the constant force approach describes drainage much better then the constant velocity approach, as numerical simulations made by Yantsios and Davis[22] and Bazhlekov *et al.*[24] indicate.

Chesters derived for the different cases expressions for the time it takes the film to reach the critical thickness for rupture; the drainage time τ_{dr} was obtained for a constant interaction force and different viscosity ratios. The coalescence probability is estimated as $P=\exp(-\tau_{dr}/\tau_{int})$,[26] where τ_{int} is the duration of the collision. For simple shear flow, this value is of the order $1/\dot{\gamma}$, where $\dot{\gamma}$ is the shear rate. This time depends on the hydrodynamic interactions during the collision and can be obtained more accurately from a trajectory analysis.[27]

To measure the coalescence probability and coalescence rate, two different approaches are used. In the first approach one directly observes two colliding droplets and their trajectories starting at different positions.[7,8,14,16,28] All the closed trajectories (coalescence) can be obtained, which results in a direct determination of the coalescence probability for droplets with given sizes. These experiments also reveal the development of the film thickness and the deformation of the droplets as a function of the interparticle distance and flow. The measured trajectories are compared with calculated ones[8,14] and provide the interaction time and the coalescence probability.

In the second approach the droplet size distribution as a function of time is measured.[9–11,15,17,29] From the time evolution of the size distribution the coalescence probability can be determined. In contrast to the two-droplets experiment this approach does not show the details of the collision but can be applied at high concentrations of the dispersed phase where one has to deal with many droplet collisions and interactions. A collision model is needed to correlate the (averaged) coalescence efficiency with the measured evolution. Mostly the Smoluchowski expression for the collision rate is used. The moments of the size distribution are measured as a function of time and the population balance equation (Smoluchowski's equation) is solved to predict the moment development.[15,30–33] The balance includes apart from the size distribution, an expression for the coalescence probability as function of the droplet sizes and the initial collision geometry. The right probability model provides the best correlation between the experimental and modeled data. However, an analytical solution for the set of moment equations depends on the coalescence frequency and the closure to obtain the finite set of equations. The size distribution of the droplets is often simplified to a log-normal,[9] or even monodisperse[17] distribution to interpret the experimental data.

Here we consider the evolution of the full size distribution. The study deals with water-in-oil emulsions under simple shear flow. The development of the size distribution is monitored as a function of time for several volume fractions and shear rates. Only low shear rates are considered to avoid breakup of the droplets.

The paper is organized as follows. In Sec. II the coalescence efficiency and coalescence rate for a pair of droplets in simple shear flow will be discussed. The models for the drainage time are considered together with the simple approach for the duration time of droplets interaction. The expression connecting the experimental data with the model predictions is derived for emulsions with an arbitrary size distribution. In Sec. III the experimental method to obtain the evolution of the size distribution is discussed and the experimental results are shown. In Sec. IV the correlation of experimental data with various models is discussed and some conclusions are presented.

II. THEORY

Collisions between two emulsion droplets in simple shear flow occur as they move along nearby streamlines with different velocities. During such a collision a thin liquid film is formed, which drains under the imposed hydrodynamic and van der Waals forces. Destabilization of the film by thermodynamic fluctuations leads to its rupture and the two droplets merge together. The film thickness, at which rupture occurs, depends on the size of the colliding droplets and varies from hundredths of a nanometer up to several nanometers.[19] Because the coalescence process is driven by both hydrodynamic and thermodynamic interactions, the rate of coalescence depends on parameters as the viscosity of the droplet μ_d and the continuous phase μ_c, the surface tension σ (and its gradient if surfactant is present), the size of the droplets, type, and intensity of flow. All of these parameters can be rearranged in a number of dimensionless parameters to describe the droplet deformation under flow and the kinetics of the coalescence process.

The capillary number Ca, being the ratio between applied and interfacial stresses, is the main parameter controlling the shape of a droplet. The droplet remains spherical when this number is much smaller than unity. The critical value, Ca_{cr}, at which breakup of a droplet occurs, is usually of the order of unity. This value depends on the type of flow, size of the droplet, and the viscosity of the fluids. For simple

shear flow $Ca=\mu_c\dot{\gamma}r/\sigma$ where $\dot{\gamma}$ is the rate of shear and r the radius of the droplet. If the viscosity ratio $\lambda=\mu_d/\mu_c$ is smaller than one the critical condition for stable droplets is $Ca_{cr}\sim 0.05/\lambda^{2/3}$ as was estimated theoretically by Batchelor and Green[34] and also obtained from experimental observations.[35] In moderate shear flow when the shear stress imposed on the droplet by the flow is much smaller then the interfacial stress, $Ca \ll Ca_{cr}$, no breakup occurs and the evolution of the size distribution of the droplets is controlled by the coalescence process.

In this paper we study the evolution of the size distribution for $Ca \ll Ca_{cr}$ to obtain the efficiency of the coalescence process and to compare it with the theoretical models proposed in literature.

The coalescence frequency or rate $\dot{N}_{cc}(v,w)$ between droplets of volume v and w is usually described by the product of collision frequency $\dot{N}_c(v,w)$ and coalescence probability $P_c(v,w)$.[19] The collision frequency is controlled by the shear rate $\dot{\gamma}$ and the volume fraction ϕ of the droplets in the emulsion. The coalescence probability depends on the interaction time between the colliding droplets, and the drainage time of the liquid film formed between them.

A. Coalescence frequency

Considering droplets in a simple shear flow, the number of collisions per unit volume during dt between droplets with a volume in $(v,v+dv)$ and a volume in $(w,w+dw)$ can be expressed in differential form as

$$\frac{\partial \dot{N}_c(v,w,\varphi_o,\vartheta_o)}{\partial\Omega} d\Omega\, dv\, dw\, dt, \tag{1}$$

where ϑ_0 denotes the initial azimuth angle between the velocity direction, $\mathbf{x}_1$, and the center-to-center vector $\mathbf{q}_{vw}$ of the two colliding droplets at the start of the collision, see Fig. 1, and φ_0 is the initial polar angle between the gradient direction, $\mathbf{x}_2$, and the projection of the vector $\mathbf{q}_{vw}$ on the $\mathbf{x}_2$-$\mathbf{x}_3$ plane. Ω is a solid angle.

Assuming affine motion of the droplets, the differential collision rate $\partial\dot{N}_c/\partial\Omega$ is simply given by

$$\frac{\partial \dot{N}_c(v,w,\varphi_o,\vartheta_o)}{\partial\Omega} = -\frac{1}{2}\dot{\gamma} q_{vw}^3 n(v) n(w) \cos\varphi_o \sin 2\vartheta_o \tag{2}$$

if

$$-\pi/2 < \varphi_o < \pi/2 \;\&\; \pi/2 < \vartheta_o < \pi \quad \text{(region I)},$$
$$\pi/2 < \varphi_o < 3\pi/2 \;\&\; 0 < \vartheta_o < \pi/2 \quad \text{(region II)}, \tag{3}$$

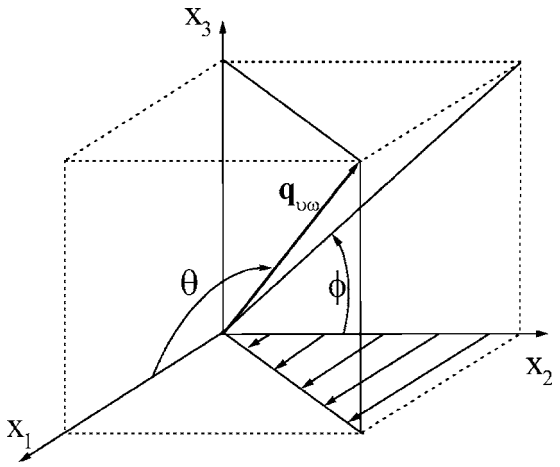

FIG. 1. The collision geometry.

otherwise $\partial\dot{N}_c/\partial\Omega$ is zero. Here $n(v)dv$ is the number density of drops with a volume between v and $v+dv$. The differential number of collisions per unit time leading to coalescence is now defined as

$$\frac{\partial \dot{N}_{cc}(v,w,\varphi_o,\vartheta_o)}{\partial\Omega} = P_c(v,w,\varphi_o,\vartheta_o)\frac{\partial \dot{N}_c(v,w,\varphi_o,\vartheta_o)}{\partial\Omega}, \tag{4}$$

where $P_c(v,w,\varphi_o,\vartheta_o)$ is the coalescence probability for a droplet with volume v with a drop with volume w, if their center-to-center vector is initially oriented along the (ϑ_o,φ_o) direction. Integrating over the solid angle Ω yields for the coalescence rate,

$$\begin{aligned}\dot{N}_{cc}(v,w) &= \int \frac{\partial \dot{N}_{cc}(v,w,\varphi_o,\vartheta_o)}{\partial\Omega} d\Omega \\ &= -\frac{1}{2}\dot{\gamma} q_{vw}^3 n(v) n(w) \int\int P_c(v,w,\varphi_o,\vartheta_o)\cos\varphi_o \\ &\quad \times \sin 2\vartheta_o\, d\varphi_o \sin\vartheta_o\, d\vartheta_o.\end{aligned} \tag{5}$$

Defining P_c' as the solid angle averaged value for P_c,

$$P_c'(v,w) = \frac{\displaystyle\int_{\pi/2}^{\pi}\left[\int_{-\pi/2}^{\pi/2} P_c(v,w,\varphi_o,\vartheta_o)\cos\varphi_o\, d\varphi_o\right]\sin 2\vartheta_o \sin\vartheta_o\, d\vartheta_o}{\displaystyle\int_{-\pi/2}^{\pi/2}\cos\varphi_o\, d\varphi_o \int_{\pi/2}^{\pi}\sin 2\vartheta_o \sin\vartheta_o\, d\vartheta_o}, \tag{6}$$

where only integration over region I is necessary due to the symmetry of the problem, one obtains for the collision rate $\dot{N}_c$ and the coalescence rate $\dot{N}_{cc}$,

$$\dot{N}_c(v,w) = \tfrac{4}{3}\dot{\gamma} q_{vw}^3 n(v) n(w) \quad \text{and}$$
$$\dot{N}_{cc}(v,w) = \dot{N}_c(v,w) P_c'(v,w), \tag{7}$$

respectively.

The start of a collision event is defined as the moment at which the two droplets become in contact; then q_{vw} is equal to

$$q_{vw} = r_v + r_w = \left(\frac{3}{4\pi}\right)^{1/3} (v^{1/3} + w^{1/3}), \tag{8}$$

where r_v and r_w are the radii of colliding droplets, and the collision rate becomes

$$\dot{N}_c(v,w) = \frac{\dot{\gamma}}{\pi}(v^{1/3} + w^{1/3})^3 n(v) n(w). \tag{9}$$

B. Population balance equation

The evolution of the droplet size distribution is described by the population balance equation. This equation reflects the rate of change of the number of droplets $n(v,t)dv$ having a volume between v and $v+dv$ due to coalescence and breakup of droplets. Assuming only binary droplet collisions, the population balance for coalescence can be written as

$$\frac{\partial n(v,t)}{\partial t} = \frac{1}{2}\int_0^v \dot{N}_{cc}(v-w,w)dw - \int_0^\infty \dot{N}_{cc}(v,w)dw, \tag{10}$$

where $\dot{N}_{cc}(v,w)$ is the coalescence rate discussed in previous subsection. The first term on the right-hand side of Eq. (10) describes the increase of number of droplets with volume v due to coalescence of two smaller droplets with volume w and $v-w$, respectively. The second term on the right-hand side describes the decrease of number of droplets with volume v, due to their coalescence with other droplets in the emulsion.

The total number of droplets per unit volume is obtained from the integration of the size distribution (its zeroth moment),

$$N(t) = \int_0^\infty n(v,t)dv, \tag{11}$$

while the volume fraction ϕ of droplets in the emulsion, which is constant, is given by the first moment,

$$\phi = \int_0^\infty v n(v,t)dv = \langle v \rangle N(t). \tag{12}$$

In the Appendix the time rate of change of the total number of droplets is calculated by integrating Eq. (10) over the volume v,

$$\dot{N} = \frac{d}{dt}\int_0^\infty n(v,t)dv = -\frac{\dot{\gamma}}{\pi}\langle\langle P_c\rangle\rangle \phi N\left(1 + 3\frac{\langle v^{1/3}\rangle\langle v^{2/3}\rangle}{\langle v\rangle}\right), \tag{13}$$

where the coalescence probability averaged over the number of collisions per unit time, $\langle\langle P_c\rangle\rangle$, is defined by

$$\langle\langle P_c\rangle\rangle \equiv \frac{\int_0^\infty \int_0^\infty P_c'(v,w)\dot{N}_c(v,w)dvdw}{\int_0^\infty \int_0^\infty \dot{N}_c(v,w)dvdw}. \tag{14}$$

Note that $\langle\cdot\rangle$ denotes averaging over the size distribution $n(v,t)$, while $\langle\langle\cdot\rangle\rangle$ denotes averaging over the collision rate $\dot{N}_c$, which is given by Eq. (9).

Experimentally we obtain for given ϕ and $\dot{\gamma}$ the time evolution of $n(v,t)$ and $N(t)$. Given a model for $P_c(v,w,\varphi_o,\vartheta_o)$ one can calculate $\langle\langle P_c\rangle\rangle$ with Eq. (14). Although the experimentally obtained distribution $n(v,t)$ is used for this calculation, we will call it $\langle\langle P_c\rangle\rangle_{\text{mod}}$ which will be compared with the experimentally obtained value,

$$\langle\langle P_c\rangle\rangle = \frac{-\dot{N}(t)}{\phi N(t)}\frac{\pi}{\dot{\gamma}}\left(1 + 3\frac{\langle v^{1/3}\rangle\langle v^{2/3}\rangle}{\langle v\rangle}\right)^{-1}, \tag{15}$$

which we will call $\langle\langle P_c\rangle\rangle_{\text{exp}}$. The better the model the closer the points will lay to the line

$$\langle\langle P_c\rangle\rangle_{\text{mod}} = \langle\langle P_c\rangle\rangle_{\text{exp}} \tag{16}$$

if one plots $\langle\langle P_c\rangle\rangle_{\text{mod}}$ against $\langle\langle P_c\rangle\rangle_{\text{exp}}$.

The analysis described above is an integral formalism that we will use to compare several models for the two-droplet coalescence probability with our experimental results. In this approach one does not need to solve the full population balance, Eq. (10), to test the models for $P_c(v,w,\varphi_o,\vartheta_o)$. The use of the experimental size distribution in calculating $\langle\langle P_c\rangle\rangle_{\text{mod}}$ provides a way to relate the experimentally inaccessible $P_c(v,w,\varphi_o,\vartheta_o)$ to the experimentally accessible moments ($\langle v^{1/3}\rangle$, $\langle v^{2/3}\rangle$, $\langle v\rangle$), and the relative rate of change of the total number of droplets, $\dot{N}(t)/N(t)$. The advantage of this approach is that the size distribution is used only as a weighing function, while the population balance method is more sensitive to details in the dynamics of the size distribution.

C. Coalescence probability

Following Ref. 19 we assume that the coalescence probability, $P_c(v,w,\varphi_0,\vartheta_0)$, is controlled by two characteristic times: the duration of the collision, τ_{int}, and the drainage time of the thin liquid film between droplets, τ_{dr}. Furthermore it has been assumed that the drainage time does not interfere with the collision time of droplets, and therefore,

$$P_c(v,w,\vartheta_0,\varphi_0) = \exp\left(\frac{-\tau_{\text{dr}}(v,w)}{\tau_{\text{int}}(\vartheta_o,\varphi_o)}\right). \tag{17}$$

The value of $\tau_{\text{dr}}(v,w)$ depends on the size of the droplets and $\tau_{\text{int}}(\vartheta_o,\varphi_o)$ depends on the initial orientation of the center-to-center vector between the colliding droplets. As it was

TABLE I. Drainage time τ_{dr} and initial film thickness h_o for the constant force approach.

Model	τ_{dr}	h_o	λ
FMI_d	$(3\mu_c R/2\sigma)\ln(h_o/h_{cr})$	$\frac{3}{2}RCa$	$\lambda \ll 1$
FMI_{nd}	$(C\lambda\mu_c R^{3/2}/F)(h_o^{1/2}-h_{cr}^{1/2})$	$\frac{3}{2}RCa$	$\lambda \ll 1$
PMI_d	$(\pi\lambda\mu_c\sqrt{F}/2(2\pi\sigma/R)^{3/2})(h_{cr}^{-1}-h_o^{-1})$	$(\frac{3}{16})^{1/4}R\sqrt{\lambda}Ca^{3/4}$	$\lambda \sim 1$
FII_d	$(3\mu_c R^2 F/8\pi\sigma^2)(h_{cr}^{-2}-h_o^{-2})$	$R(\frac{3}{2}Ca)^{2/3}$	$\lambda \gg 1$
FII_{nd}	$(6\pi\mu_c R^2/F)\ln(h_o/h_{cr})$	$R(\frac{3}{2}Ca)^{2/3}$	$\lambda \gg 1$

shown previously by a trajectory analysis,[27] this assumption is valid only in the limit of low viscosity ratio, $\lambda \to 0$. For other values of λ the interaction time is also a function of the droplet size. In simple shear flow when $Re \ll 1$ the drainage time is controlled by the viscosity ratio λ, the capillary number Ca, the ratio of the undeformed droplets radii, and the ratio of the van der Waals forces to lubrication forces, $A/(\sigma R^2)$, where A is the Hamaker constant and $R=1/(d_v^{-1}+d_w^{-1})$ is the reduced radius $[d_v=(6v/\pi)^{1/3}]$.[27] The values of these dimensionless numbers control not only the drainage time, but also the deformation of the interfaces within the region of contact. Estimating the influence of all these parameters under the assumption of a flat film in the inner region of deformation, Chesters[19] arrived at different expressions for the drainage time, depending on the properties of the interface. These expressions are used in the calculation of $\langle\langle P_c\rangle\rangle_{mod}$ [Eq. (14)] and are listed in Table I.

Here FMI, PMI, and FII stands for fully mobile interface, partially mobile, and fully immobile interfaces, respectively. Models for deformable and nondeformable interfaces are denoted by the subscripts d and nd. $F=6\pi\mu_c\dot{\gamma}R^2$ is the Stokes drag force, $C=11.7$ is a constant, and h_0 is the initial thickness of the film. The critical value for the film thickness at rupture is $h_{cr}=(AR/4\pi\sigma)^{1/3}$. Details can be found in Ref. 19.

The interaction time is determined by the flow field and should scale with $1/\dot{\gamma}$. Moreover, it depends on the trajectories of the colliding droplets. Previous investigations[36,37] have shown that these trajectories and the interaction time strongly depend on the van der Waals force, the hydrodynamic interaction, and the deformation of the droplets in the contact region. However, as we are interested in the scaling behavior of the process, we consider touching drops which do not move along the center-to-center vector $\mathbf{q}_{vw}$ during the collision. Hence in simple shear flow the trajectory is given by $d\varphi/dt=0$ and $d\vartheta/dt=-\dot{\gamma}\cos\varphi\sin^2\vartheta$.[27] By integration of the last equation one obtains the interaction time,

$$\tau_{int}(\vartheta_0,\varphi_0) = -\frac{2\cot(\vartheta_0)}{\dot{\gamma}\cos(\varphi_0)}. \tag{18}$$

In the derivation of Eq. (18) it has been assumed that, if no coalescence occurs, the droplets will separate when $\vartheta=-\vartheta_0$.

With the expressions for the drainage and interaction time we can calculate $P_c(v,w,\vartheta_o,\varphi_o)$. Since in our case $h_0 \gg h_{cr}$, the FMI_{nd}, PMI_d, and FII_d models for $P_c(v,w,\vartheta_o,\varphi_o)$ can be represented by the general expression,

$$P_c(v,w,\vartheta_o,\varphi_o) = \exp\left(\left(\frac{R}{R_o}\right)^{\alpha}\left(\frac{\dot{\gamma}}{\dot{\gamma}_o}\right)^{\beta}\tan(\vartheta_o)\cos(\varphi_o)\right), \tag{19}$$

where parameters α, β, R_o, and $\dot{\gamma}_o$ depend on the model for the drainage time, see Table II.

We will use this expression for $P_c(v,w,\vartheta_o,\varphi_o)$ to obtain the best correlation between the model and the experimental data using α, β, and R_o as fit parameters.

III. EXPERIMENT

A. System

The choice of liquids for the dispersed and the continuous phases of the emulsion was determined by two criteria: (a) sedimentation/creaming should be prevented by density matching of the phases; (b) the refractive index of the dispersed phase should be close to the value of the continuous phase to enable measurement of the coalescence in the bulk of the emulsion.

To make such an emulsion, silicon oil was used as the continuous phase, whereas the dispersed phase was prepared as a mixture of 1,3-butanediol, hexylene glycol (ex-Merck) and double purified water (Millipore system with conductivity less than $1\times10^{-6}\ \Omega^{-1}\,cm^{-1}$) in volume proportions of 1%, 61%, and 38%, respectively. The difference of the refractive indices between the phases was $\Delta n=0.0035$ at 23 °C. The density difference was $\Delta\rho=0.0001$ g/ml (Mettler DA-200 density meter). The matching conditions $(\Delta n,\Delta\rho)$ slightly depend on the temperature of the emulsion.

Viscosity measurements of the separate phases were performed using a Haake viscosimeter with a plate-plate geometry and indicated Newtonian behavior within the examined shear rate range ($\dot{\gamma}=0.01-10\ s^{-1}$). The viscosities of the continuous and dispersed phases were 2600 and 12.4 mPa s, respectively, giving a viscosity ratio, $\lambda=\eta_d/\eta_c$, of 0.005. In this limit, as it was mentioned above, the critical capillary number, Ca_{cr}, for droplets in shear flow approximately equals to 2.

TABLE II. Values of the parameters in Eq. (19) for three of the models.

Model	α	β	R_o	R_o (mm)	$\dot{\gamma}_o$
FMI_{nd}	5/2	0	$(12\pi/C\lambda)^{2/5}(2\sigma/3\mu_c\dot{\gamma}_o)^{1/5}$	3750	1
PMI_d	13/6	3/2	$(4(2\pi\sigma)^{3/2}/\pi\mu_c\dot{\gamma}_o\lambda\sqrt{6\pi\mu_c\dot{\gamma}_o})^{6/13}(A/8\pi\sigma)^{2/13}$	0.382	1
FII_d	10/3	2	$(16\sigma^2/9\mu_c^2\dot{\gamma}_o^2)^{3/10}(A/8\pi\sigma)^{1/5}$	0.0042	1

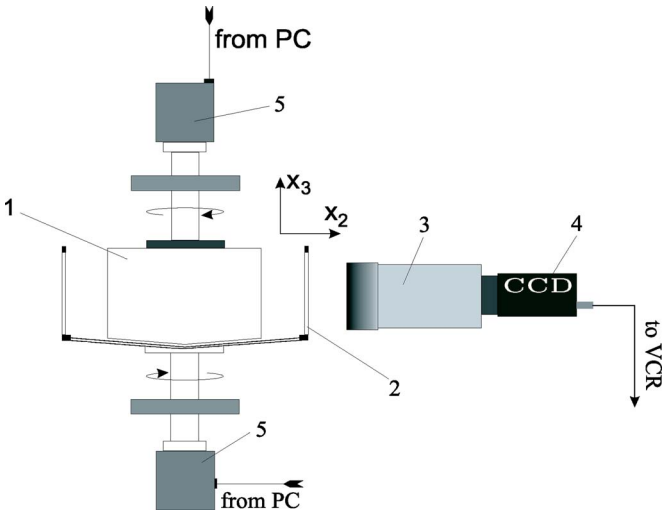

FIG. 2. The experimental setup. 1: inner cylinder; 2: outer cylinder; 3: microscope; 4: CCD camera; and 5: motors to drive inner and outer cylinders.

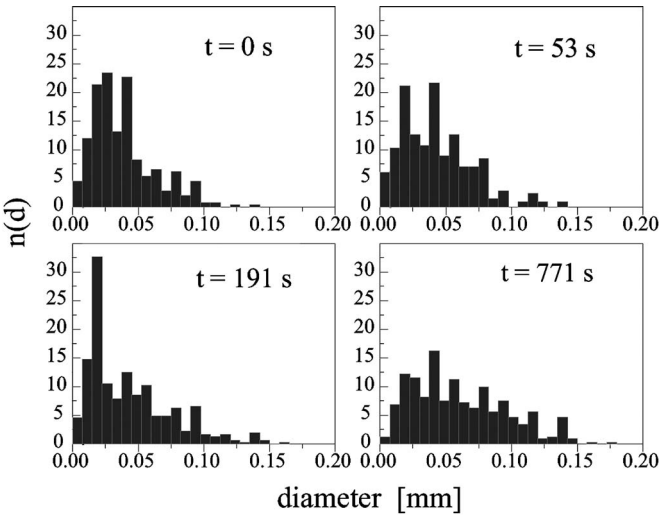

FIG. 3. The size distribution for $\phi=5\%$ and $\dot{\gamma}=0.2\ s^{-1}$ at different times after start up: 0, 53, 191, and 771 s.

The value of the interfacial tension, σ, was obtained using the retardation technique.[38] The deformation of the droplets $D=(L-B)/(L+B)$ (where L is the longest diameter of the droplet cross section and B is the perpendicular diameter) in a steady shear flow was measured as a function of the shear rate. The small deformation theory[39] predicts a linear relationship between the steady-state deformation and the capillary number at low shear rates: $D\approx Ca(16+19\lambda)/(16+16\lambda)$. This resulted in $\sigma=7.10\pm0.25$ mN/m.

In the experiments the volume fraction was in the range of 2%–14%.

B. Experimental setup

The Couette cell used for the experiments (see Fig. 2) was the same as used in a previous study.[14] Two counter-rotating cylinders provide the shear flow in the gap between them. The inner cylinder is made from aluminium, whereas the outer cylinder is made from glass to allow optical access with a microscope. The radii of inner and outer cylinders are 40 and 50 mm, respectively. The height of the gap is 50 mm. The amount of sample needed is about 120 ml. The rotational speed of each cylinder is independently controlled by a personal computer, the shear rate ranges from 0.01 to 93 s^{-1}, while the position of the stagnant layer in the gap can be varied independently from the rate of shear.

A long working distance microscope (Olympus SZX9) has been used to observe the droplets under shear flow. The microscope is mounted in such a way that its optical axis lies along the velocity gradient direction of the flow and the focal plane of the microscope is fixed at the stagnant layer. A charge-coupled device (CCD) video camera (Sony XC-75/75CE) was attached to the video port of the microscope to collect images of the emulsion for further analysis. During the experiments the emulsion was recorded continuously.

Due to the nearly perfect matching of the refractive indexes ($\Delta n=0.0035$) the droplets in the focal plane are visible without large attenuation by the droplets moving between the stagnant layer and the outer cylinder.

C. Preparation, method, and procedure

To prepare the emulsion the shear cell has been filled with the silicon oil. Subsequently the aqueous phase was injected at a rate of 1 ml/min, while the shear rate was 5 s^{-1}. When the necessary amount of the dispersed phase had been injected the rate of shear was increased to 92 s^{-1} to produce a homogeneous emulsion with small droplets due to the breakup process. After 10 min of shearing the coalescence and breakup were in balance and the morphology did not change anymore. Next the shear flow was stopped, and the elongated droplets retracted to their spherical shapes. During this process capillary breakup also occurred, further reducing the average droplet size to values between 0.03 and 0.10 mm.

The development of the emulsion's morphology was recorded on videotape. The size distribution was determined by counting 300 to 400 droplets, collected in short time intervals of about 20 s, and assembling a sorted list of diameters $\{x_1 \ldots x_n \ldots x_M\}$ with $x_n \leqslant x_{n+1}$. The moments of the size distribution $\langle x\rangle$, $\langle x^2\rangle$, and $\langle x^3\rangle$ were calculated from this list using

$$\langle x^p\rangle = \frac{1}{M}\sum_{n=1}^{M}(x_n)^p, \tag{20}$$

where M is the number of diameters in the list. The total number N of droplets per unit volume was obtained from

$$N = \frac{6\phi}{\pi\langle x^3\rangle}. \tag{21}$$

The size distribution at a certain time can be constructed from the list mentioned above. As an example the evolution of this distribution for an emulsion with a volume fraction $\phi=5\%$ at $\dot{\gamma}=0.2\ s^{-1}$ is represented in Fig. 3. To obtain more smooth distributions, the cumulative distributions (Fig. 4)

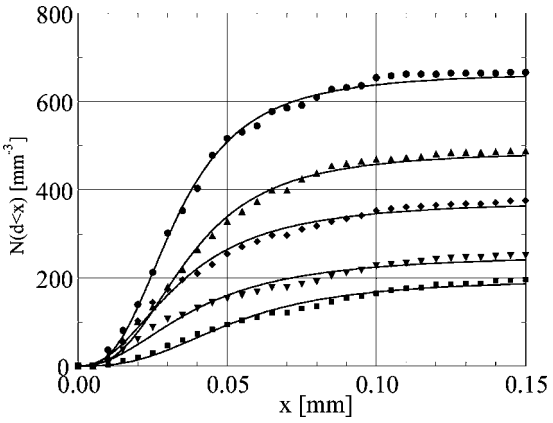

FIG. 4. The cumulative size distribution for $\phi=5\%$ and $\dot{\gamma}=0.2\ s^{-1}$ at different times after start up; from top down: 0, 53, 191, 402, and 771 s. The curves are a fit to the experimental results (points): $F(x)=N(1+(a/x_m)^b)/(1+(a/x)^b)$.

have been constructed by plotting the number of droplets with diameter d smaller than diameter x_n, $N(d<x_n)$, against x_n from the sorted list, using a bin width of 5 μm. The function

$$F(x)=\begin{cases} N[1+(a/x_m)^b]/[1+(a/x)^b], & x<x_m, \\ N, & x\geqslant x_m, \end{cases} \tag{22}$$

has been fitted to these cumulative distributions, yielding values for N, a, b, and x_m. These numbers will be used as the characteristic parameters of the size distribution in the calculation of $\langle\langle P_c\rangle\rangle_{\mathrm{mod}}$. By plotting the plateau values from Fig. 4 as a function of time, one obtains a graph of $N(t)$ (see Fig. 5; $\phi=5\%$, $\dot{\gamma}=0.2\ s^{-1}$). From $N(t)$ the rate $K(t)=-d\ln[N(t)/N_o]/dt$ can be determined. Here $N_o=N(t=0)$. The result is presented in the same figure.

Values for $\langle\langle P_c\rangle\rangle_{\mathrm{exp}}$ [Eq. (15)] were calculated from $K(t)$ and $\langle x\rangle$, $\langle x^2\rangle$, and $\langle x^3\rangle$ as obtained from Eq. (20). The corresponding values for $\langle\langle P_c\rangle\rangle_{\mathrm{mod}}$ [Eq. (14)] have been determined using the size distribution $n(v,t)$ as calculated from the cumulative distribution [Eq. (22)],

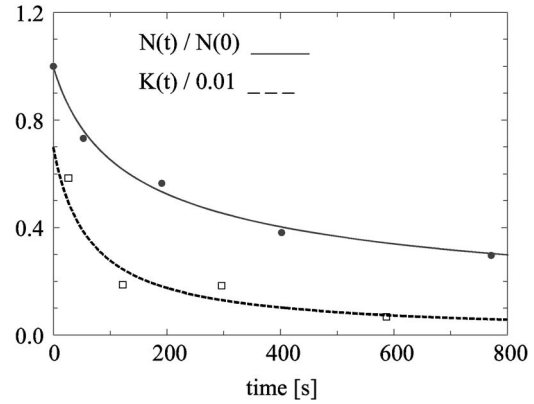

FIG. 5. The total number of droplets $N(t)$ as a function of time (upper curve) and $K(t)=d\ln[N_o/N(t)]/dt$ (lower curve); the measuring points are obtained from the plateau values in Fig. 4.

$$n(v,t)=\frac{dF(x)}{dx}\frac{dx}{dv}, \tag{23}$$

and one of the expressions for $P_c(v,w,\vartheta_o,\varphi_o)$ given in Sec. II.

D. Results

To compare the macroscopic coalescence probability $\langle\langle P_c\rangle\rangle$ with the microscopic two-particle coalescence probability $P_c(v,w,\vartheta_o,\varphi_o)$ under various experimental conditions, the evolution of the emulsion morphology has been measured for several volume fractions, $\phi=2\%$, 5%, 10%, and 14%, and rates of shear, $\dot{\gamma}=0.1$, 0.2, 0.5, and 10.0 s^{-1}. The results have been listed in Table III, where Δt is the time interval between two measurements. In the last column the value for $\langle\langle P_c\rangle\rangle_{\mathrm{exp}}$ has been given as calculated from the data listed in the table. Before model predictions of $\langle\langle P_c\rangle\rangle$ could be calculated, the values for a, b, and x_m were determined such that the values for $\langle x\rangle$, $\langle x^2\rangle$, and $\langle x^3\rangle$ of the cumulative distribution Eq. (22) were in agreement with the ones calculated using Eq. (20). Next $\langle\langle P_c\rangle\rangle_{\mathrm{mod}}$ could be calculated for the models listed in Table I. In these models the parameter values were $\eta=2.6$ Pa s, $\lambda=0.005$, and $\sigma=0.007$ N/m, while the Hamaker constant was taken as $A=5\times10^{-21}$ J. All the models, except the FII_d model, overestimate the observed $\langle\langle P_c\rangle\rangle_{\mathrm{exp}}$ significantly: $\langle\langle P_c\rangle\rangle_{\mathrm{mod}}\simeq 1$. The results for the FII_d model are presented in Fig. 6, where $\langle\langle P_c\rangle\rangle_{\mathrm{mod}}$ has been plotted against $\langle\langle P_c\rangle\rangle_{\mathrm{exp}}$ (open symbols).

The horizontal error bars in this and the following diagrams of $\langle\langle P_c\rangle\rangle_{\mathrm{mod}}$ against $\langle\langle P_c\rangle\rangle_{\mathrm{exp}}$ were obtained from estimating the largest and the smallest values of $K(t)$: $[N(t)-N(t+\Delta t)]/[N(t+\Delta t)\Delta t]$ and $[N(t)-N(t+\Delta t)]/[N(t)\Delta t]$, respectively. As previously, Δt denotes the time interval between two measurements. The vertical error bars were estimated from the quality of the fit to the cumulative size distribution $F(x)$ [Eq. (22)] by comparing this fit to the best fit with a fixed value for $x_m=20\langle x\rangle$.

In our experiments we were able to vary $\langle\langle P_c\rangle\rangle_{\mathrm{exp}}$ over three orders of magnitude. The model predictions in this range are within the same order of magnitude as the observed probabilities.

Because of the known value for the Hamaker constant, the coalescence probability, Eq. (19), was tested with $\alpha=10/3$ and $\beta=2$ taken in accordance with the FII_d model. However, R_o was used as a fitting parameter. The best fit was obtained for $R_o=0.0121$ mm instead of 0.0042 mm, as listed in Table II. The result of the fitting procedure is shown in Fig. 6 by the closed symbols. For the fully immobile deformable interface model, the corresponding value for the Hamaker constant should be about 10^{-18} J. When the PMI_d is used, the result of fitting is displayed in Fig. 7. Here the open symbols represent the data for $R_o=0.382$ mm while the closed symbols represent the data obtained by fitting R_o (0.0101 mm for the best fit), which implies a Hamaker constant of 10^{-31} J. Without adjustment of R_o one observes indeed overestimation of the experimental coalescence probability by the PMI_d model. In case of the $\mathrm{FMI}_{\mathrm{nd}}$ model, the shear rate dependence of the coalescence probability ($\beta=0$)

TABLE III. Experimental results.

No.	ϕ (%)	$\dot{\gamma}$ (s^{-1})	Δt, time interval (s)	$\langle x^3\rangle$[a] (mm^3)	K (s^{-1})	$1+3\langle x\rangle\langle x^2\rangle/\langle x^3\rangle$	$\langle\langle P_c\rangle\rangle_{exp}$
1	2	0.11	0–300	0.000 24	0.001 66	3.381	0.6996
		0.11	300–600	0.000 35	0.000 80	3.344	0.3420
2		1.00	0–60	0.000 56	0.003 40	2.864	0.1863
		1.00	60–276	0.000 64	0.000 45	2.866	0.0248
3		1.00	0–457	0.000 73	0.001 05	2.825	0.0586
4		10.0	0–124	0.000 19	0.000 72	3.043	0.0037
		10.0	124–379	0.000 24	0.000 89	2.922	0.0048
5	5	0.11	0–360	0.000 10	0.002 53	3.009	0.4811
		0.11	360–720	0.000 20	0.001 35	2.688	0.2873
6		0.11	0–154	0.000 09	0.003 20	2.711	0.6747
		0.11	154–451	0.000 08	0.000 92	2.804	0.1880
7		0.11	0–835	0.000 09	0.000 88	2.934	0.1705
8		0.20	0–53	0.000 17	0.005 85	2.716	0.6766
		0.20	53–191	0.000 22	0.001 89	2.610	0.2277
		0.20	191–402	0.000 32	0.001 84	2.524	0.2287
		0.20	402–771	0.000 43	0.000 68	2.707	0.0791
9		0.50	0–114	0.000 33	0.005 01	2.961	0.2125
		0.50	114–363	0.000 46	0.000 66	3.043	0.0275
10		0.50	0–200	0.000 16	0.001 24	3.069	0.0509
		0.50	200–500	0.000 20	0.001 16	3.107	0.0469
11		10.0	0–87	0.000 13	0.000 64	3.316	0.0012
12	10	0.11	0–405	0.001 55	0.002 85	3.319	0.2449
		0.11	405–870	0.003 82	0.001 93	3.303	0.1668
13		0.19	0–387	0.002 97	0.000 81	2.805	0.0477
		0.19	387–644	0.003 88	0.000 87	2.840	0.0508
14	14	0.50	0–100	0.000 48	0.007 66	2.875	0.1195
		0.50	100–200	0.000 79	0.003 11	2.817	0.0496
		0.50	200–400	0.001 11	0.001 62	2.738	0.0266

[a]Note that $N=6\phi/\pi\langle x^3\rangle$.

is also not in agreement with the experiments. This indicates that the optimum seems to lie between the PMI and the FII models. To get an impression of the shear rate and size dependence of the coalescence probability, Eq. (19) with adjustable parameters α, β, and R_o has been fitted to the experimental data. The results are given in Fig. 8: $\alpha=1.175$ and $\beta=0.7875$ while $R_o=0.0057$ mm. However, the quality of the fit is not significantly better than in case of the FII_d model

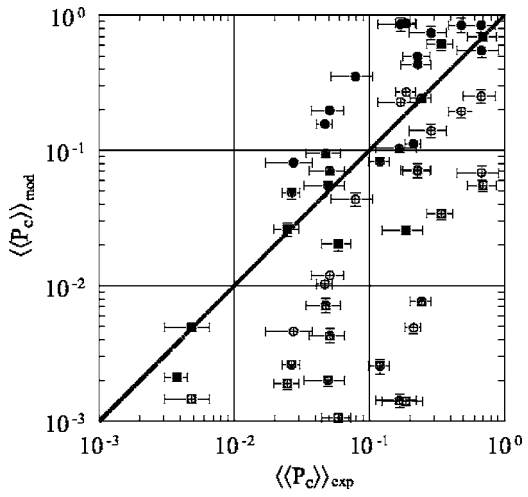

FIG. 6. $\langle\langle P_c\rangle\rangle_{mod}$ plotted against $\langle\langle P_c\rangle\rangle_{exp}$ for the FII_d model; open symbols: the model calculations with $R_o=0.0042$ mm; as calculated from the parameters in Table II; closed symbols: $R_o=0.0121$ mm, adjusted to obtain a best fit; $\phi=2\%$ (□, ■), 5% (○, ●), 10% (△, ▲), and 14% (▽, ▼).

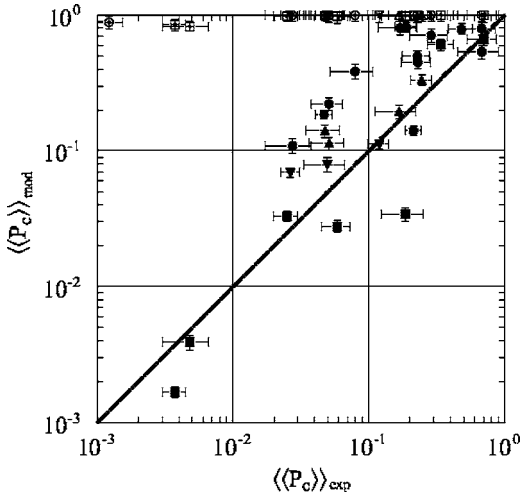

FIG. 7. $\langle\langle P_c\rangle\rangle_{mod}$ plotted against $\langle\langle P_c\rangle\rangle_{exp}$ for the PMI_d model; open symbols: the model calculations with $R_o=0.382$ mm, as calculated from the parameters in Table II; closed symbols: $R_o=0.0101$ mm, adjusted to obtain a best fit; $\phi=2\%$ (□, ■), 5% (○, ●), 10% (△, ▲), and 14% (▽, ▼).

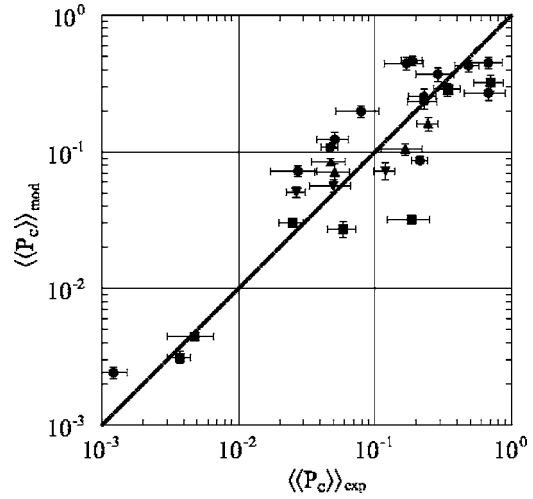

FIG. 8. $\langle\langle P_c\rangle\rangle_{\mathrm{mod}}$ plotted against $\langle\langle P_c\rangle\rangle_{\mathrm{exp}}$ for the best fit to Eq. (19): $\alpha=1.175$, $\beta=0.7875$, and $R_o=0.0057$; $\phi=2\%$ (■), 5% (●), 10% (▲), and 14% (▼).

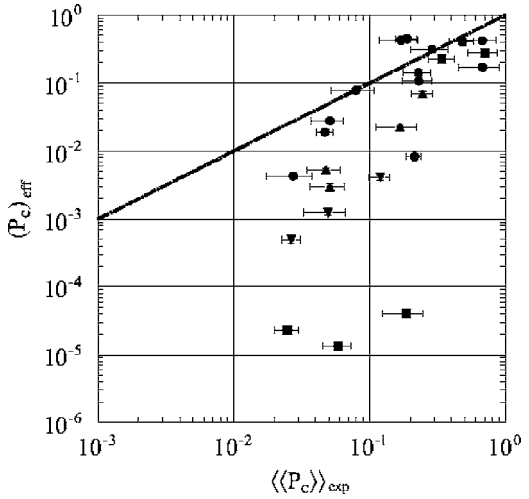

FIG. 9. $(P_c)_{\mathrm{eff}}$ plotted against $\langle\langle P_c\rangle\rangle_{\mathrm{exp}}$ using the coalescence probability based on the effective collision radius as given in Eqs. (25) and (26) with $\alpha=1.175$, $\beta=0.7875$, and $R_o=0.0057$; $\phi=2\%$ (■), 5% (●), 10% (▲), and 14% (▼).

(Fig. 6) or the PMI_d model (Fig. 7) if one optimizes the value of R_o. So α is about 2 ± 1 and β is about 1.5 ± 1.0. Independently on the model, the value for the effective coalescence radius R_o above which the probability strongly decreases is $R_o=10\pm4$ μm.

In previous articles describing the coalescence dynamics of polydisperse emulsions,[9,29,40] the coalescence probability was estimated using an averaged coalescence radius. To compare this approach with ours, we calculated the collision radius averaged over the number of collisions per unit time between drops with size v and drops with size w,

$$\langle\langle R\rangle\rangle = \frac{\int_0^\infty \int_0^\infty x_v x_w/(x_v+x_w)\dot{N}_c(v,w)dv\,dw}{\int_0^\infty \int_0^\infty \dot{N}_c(v,w)dv\,dw} = \frac{\langle x\rangle\langle x^3\rangle + \langle x^2\rangle\langle x^2\rangle}{\langle x^3\rangle + 3\langle x\rangle\langle x^2\rangle}, \tag{24}$$

where $\dot{N}_c(v,w)dv\,dw$ is defined by Eq. (9). Equation (13) is still valid for the change of the total number of droplets per unit volume, but now with

$$\langle\langle P_c\rangle\rangle = (P_c)_{\mathrm{eff}} = \exp\left(\frac{-\tau_{\mathrm{dr}}(\langle\langle R\rangle\rangle)}{\tau_{\mathrm{int}}(\dot{\gamma})}\right), \tag{25}$$

which can be estimated from the first three moments of $n(v)$. We have calculated P_c using the averaged radius $\langle\langle R\rangle\rangle$ and Eq. (19) with values for α and β as obtained from the best fit,

$$(P_c)_{\mathrm{eff}} = \exp\left(-\frac{\pi}{2}\left(\frac{\langle\langle R\rangle\rangle}{R_o}\right)^\alpha\left(\frac{\dot{\gamma}}{\dot{\gamma}_o}\right)^\beta\right), \tag{26}$$

and plotted it against $\langle\langle P_c\rangle\rangle_{\mathrm{exp}}$ (see Fig. 9). It can be concluded that for $\langle\langle P_c\rangle\rangle_{\mathrm{exp}}<0.1$ the predictions based on an effective radius $\langle\langle R\rangle\rangle$ underestimate the measured probabilities by many orders of magnitude. So it is essential to take into account the full size distribution in predicting the coalescence probability in polydisperse emulsions under shear.

IV. DISCUSSION AND CONCLUSION

The coalescence frequency in emulsions containing droplets with a low viscosity (viscosity ratio ~0.005) in simple shear flow has been investigated experimentally at several volume fractions of the dispersed phase (2%–14%) and several values of the shear rate ($0.1-10\ \mathrm{s}^{-1}$). The evolution of the size distribution was monitored to determine the average coalescence probability from the decrease of the total number of droplets. Models for two-droplet coalescence have been considered, where the probability has been expressed as $P_c=\exp(-\tau_{\mathrm{dr}}/\tau_{\mathrm{int}})$. Since the drainage time τ_{dr} in these models depends on the sizes of the two colliding droplets and the collision time τ_{int} depends on the initial orientation of the colliding droplets, the calculated coalescence probability was averaged over the initial orientation distribution and the experimentally obtained droplet size distribution. This procedure provides the averaged probability $\langle\langle P_c\rangle\rangle_{\mathrm{mod}}$ which was compared with the experimentally obtained coalescence probability $\langle\langle P_c\rangle\rangle_{\mathrm{exp}}$.

$\langle\langle P_c\rangle\rangle_{\mathrm{exp}}$ was obtained by measuring the size distribution as a function of time. These measured cumulative distributions could be described very well, in all cases, by an empirical fit function $F(x)$ [Eq. (22)]. The value of the cut-off size x_m should be significantly larger than $\langle x\rangle$ because otherwise at this point a discontinuity will occur in the size distribution $dF(x)/dx$. In all cases x_m was found to be larger than $4\langle x\rangle$ leading to a discontinuity of less than 5% of the maximum of the size distribution, which is beyond the experimental accuracy, see Fig. 4. Fitting the experimental distributions by a log-normal distribution (as done by several researchers) yielded a worse correlation between the measured and calculated coalescence probabilities, especially for longer times after start up of the flow.

From Figs. 6–8 one can observe that the volume fraction dependence is well described by the fully immobile deformable interface and partially mobile deformable interface models; the $\phi=2\%$, 5%, 10%, and 14% data show the same behavior of $\langle\langle P_c\rangle\rangle_{\mathrm{mod}}$ upon $\langle\langle P_c\rangle\rangle_{\mathrm{exp}}$. Considering the uncertainty in the plotted data the quality of the fits in Figs. 6–8 is comparable. This indicates that the interface of the droplets is hardly mobile; the partially mobile interface model holds only if one assumes a very low value for the Hamaker constant, 10^{-31} J, while the fully immobile interface model is valid if a rather high value for the Hamaker constant, 10^{-18} J, is considered. From the perspective of the used emulsions one expects a mobile interface, because no surfactants were used and the viscosity ratio, $\lambda=0.005$, was much smaller than 1. However, due to the complexity of the dispersed phase, probably one of the components also adsorbs (for a small fraction) to the interface, lowering its mobility. Another possible factor is the van der Waals interaction that has been taken into account only at the latest stage of the coalescence process; more refined modeling suggests a lowering of the coalescence probability in favor of a more mobile interface. In addition, the refractive index matching conditions may also decrease the value of the Hamaker constant.[41,42]

Independent of the chosen model we obtained a scaling of the ratio $\tau_{\mathrm{dr}}/\tau_{\mathrm{int}}$ with the rate of shear $\dot{\gamma}$, $\tau_{\mathrm{dr}}/\tau_{\mathrm{int}} \sim \dot{\gamma}^{(3/2\pm1)}$, indicating that for $\dot{\gamma}<10\ \mathrm{s}^{-1}$ the coalescence probability depends quite significantly on the rate of shear. The scaling with the reduced radius $R=x_1x_2/(x_1+x_2)$ is given by $\tau_{\mathrm{dr}}/\tau_{\mathrm{int}}\sim R^{(2\pm1)}$ with a critical collision radius of about $R_o=10\ \mu$m; i.e., the probability that droplets larger than 10 μm coalescence with each other decreases drastically with increasing droplet size. Moreover from Fig. 9 it is obvious that one must take into account the polydispersity of the droplet size to estimate the probability $\langle\langle P_c\rangle\rangle$ otherwise the predictions for probabilities below 10% are at least more than three orders of magnitude wrong.

For a single experimental run where the size distribution develops in time at fixed experimental conditions (shear rate and concentration), the experimentally obtained $\langle\langle P_c\rangle\rangle_{\mathrm{exp}}$ decreases faster with time than the calculated $\langle\langle P_c\rangle\rangle_{\mathrm{mod}}$. Such trend is visible for all series of experiments as seen in Fig. 8. This is a clear indication that the calculated coalescence probability should be modified in order to match the experimentally obtained values. A possible explanation could be the formation of a dimple in the vicinity of the contact area of the colliding droplets. This deformation occurs due to the axisymmetric lubrication pressure, which together with the van der Waals forces leads to a smaller collision rate for larger droplets.[27,43] To take such an effect into account trajectory calculations are needed, instead of the Smoluchowski collision rate approximation used in this analysis.

As mentioned above, only the appropriate model for the coalescence probability gives on the average the right correlation line $\langle\langle P_c\rangle\rangle_{\mathrm{mod}}=\langle\langle P_c\rangle\rangle_{\mathrm{exp}}$ for the different experimental conditions (shear rate, concentration, size distribution). However, there is still a lot of scattering in the data, that originates from several possible sources in both the experiments and the modeling. One is the relatively low number of droplets considered in the distributions, which affects the experimental result but also the calculations of $\langle\langle P_c\rangle\rangle_{\mathrm{mod}}$. Also the poor time resolution hampers the experimental accuracy. Improvements can be achieved, for instance, by the three-dimensional (3D) sample scanning method, recently highlighted by Caserta *et al.*[44] or by using an aerometrics phase Doppler particle analyzer.[45]

In conclusion one can state the following: (1) To predict the average coalescence probability one has to take into account the full size distribution of the droplets. (2) The coalescence process is best described by the partially mobile deformable interface or the fully immobile deformable interface model of Chesters.[19] (3) Independent of the model used it was concluded that the ratio $\tau_{\mathrm{dr}}/\tau_{\mathrm{int}}$ scales with the coalescence radius as $\tau_{\mathrm{dr}}/\tau_{\mathrm{int}}\sim R^{(2\pm1)}$ and with the rate of shear as $\tau_{\mathrm{dr}}/\tau_{\mathrm{int}}\sim\dot{\gamma}^{(3/2\pm1)}$. The critical coalescence radius R_o, above which hardly any coalescence occurs, is about 10 μm.

ACKNOWLEDGMENT

The authors acknowledge the European Community for their financial support (Project No. BE 4322).

APPENDIX: THE TOTAL NUMBER RATE

The time rate of change of the total number of drops is given by integrating Eq. (10),

$$\begin{aligned}\dot{N}&=\frac{\partial}{\partial t}\int_0^\infty n(v,t)dv\\&=\frac{1}{2}\int_0^\infty\int_0^v \dot{N}_{cc}(v-w,w)dw\,dv-\int_0^\infty\int_0^\infty \dot{N}_{cc}(v,w)dw\,dv\\&=-\frac{1}{2}\int_0^\infty\int_0^\infty \dot{N}_{cc}(v,w)dw\,dv.\end{aligned}$$

The coalescence rate $\dot{N}_{\mathrm{cc}}$ is given by Eq. (7). Thus

$$\dot{N}=-\frac{1}{2}\int_0^\infty\int_0^\infty\frac{\dot{\gamma}}{\pi}(v^{1/3}+w^{1/3})^3n(v)n(w)P_c(v,w)dw\,dv. \tag{A1}$$

Using Eq. (6) one obtains

$$\begin{aligned}\dot{N}&=-\frac{\dot{\gamma}}{2\pi}\langle\langle P_c\rangle\rangle\int_0^\infty\int_0^\infty(v^{1/3}+w^{1/3})^3n(v)n(w)dw\,dv\\&=-\frac{\dot{\gamma}}{2\pi}\langle\langle P_c\rangle\rangle\int_0^\infty\int_0^\infty(v+3v^{2/3}w^{1/3}+3v^{1/3}w^{2/3}\\&\quad+w)n(v)n(w)dw\,dv\\&=-\frac{\dot{\gamma}}{\pi}\langle\langle P_c\rangle\rangle N^2(\langle v\rangle+3\langle v^{1/3}\rangle\langle v^{2/3}\rangle),\end{aligned}$$

which leads finally with $\phi=\langle v\rangle N$ to Eq. (13),

$$\dot{N}=-\frac{\dot{\gamma}}{\pi}\langle\langle P_c\rangle\rangle\phi N\left(1+3\frac{\langle v^{1/3}\rangle\langle v^{2/3}\rangle}{\langle v\rangle}\right). \tag{A2}$$

[1] *Encyclopedia of Emulsion Technology*, edited by P. Becher (Marcel Dekker, New York, 1985), Vol. 2, p. 536.
[2] *Emulsion Polymerization and Emulsion Polymers*, edited by P. A. Lovell and M. S. El-Aasser (Wiley, New York, 1997), p. 826.
[3] *Modern Aspects of Emulsion Science*, edited by P. B. Binks (The Royal Society of Chemistry, Cambridge, 1998), p. 430.
[4] P. T. Jaeger, J. J. M. Janssen, F. Groeneweg, and W. G. M. Agterof, Colloids Surf., A **85**, 255 (1994).
[5] J. A. Wieringa, F. van Dieren, J. J. M. Janssen, and W. G. M. Agterof, Chem. Eng. Res. Des. **74**, 554 (1996).
[6] M. Minale, P. Moldenaers, and J. Mewis, Macromolecules **30**, 5470 (1997).
[7] S. Guido and M. Simeone, J. Fluid Mech. **357**, 1 (1998).
[8] H. Yang, C. C. Park, Y. T. Hu, and L. G. Leal, Phys. Fluids **13**, 1087 (2001).
[9] V. Mishra, S. M. Kresta, and J. H. Masliyah, J. Colloid Interface Sci. **197**, 57 (1998).
[10] A. Nandi, A. Mehra, and D. V. Khakhar, Phys. Rev. Lett. **83**, 2461 (1999).
[11] A. Nandi, D. V. Khakhar, and A. Mehra, Langmuir **17**, 2647 (2001).
[12] E. Klaseboer, Ph.D. thesis, Institute National Polytechnique de Toulouse, France, 1998.
[13] S. D. Hudson, B. E. Burkhart, V. P. Gopalkrishnan, A. M. Jamieson, and I. Manas-Zloczower, in *Proceedings of the XIIIth International Congress on Rheology*, Cambridge, UK, 20–25 August 2000, edited by D. M. Binding, N. E. Hudson, J. Mewis, J.-M. Piau, C. J. S. Petrie, P. Townsend, M. H. Wagner, and K. Walters (British Society of Rheology, 2000), pp. 2-88–2-90.
[14] H. Mousa, W. Agterof, and J. Mellema, J. Colloid Interface Sci. **240**, 340 (2001).
[15] H. Mousa and T. G. M. van de Ven, Colloids Surf. **60**, 19 (1991).
[16] Y. T. Hu, D. J. Pine, and L. G. Leal, Phys. Fluids **12**, 484 (2000).
[17] B. E. Burkhart, P. V. Gopalkrishnan, S. D. Hudson, A. M. Jamieson, M. A. Rother, and R. H. Davis, Phys. Rev. Lett. **87**, 098304 (2001).
[18] M. Smoluchowski, Z. Phys. Chem., Stoechiom. Verwandtschaftsl. **92**, 129 (1917).
[19] A. K. Chesters, Chem. Eng. Res. Des. **69**, 259 (1991).
[20] R. H. Davis, J. A. Schonberg, and J. M. Rallison, Phys. Fluids A **1**, 77 (1989).
[21] S. Abid and A. K. Chesters, Int. J. Multiphase Flow **20**, 613 (1994).
[22] S. G. Yantsios and R. H. Davis, J. Colloid Interface Sci. **144**, 412 (1991).
[23] A. Saboni, C. Gourdon, and A. K. Chesters, J. Colloid Interface Sci. **175**, 27 (1995).
[24] I. B. Bazhlekov, A. K. Chesters, and F. N. van de Vosse, Int. J. Multiphase Flow **26**, 445 (2000).
[25] M. A. Rother, A. Z. Zinchenko, and R. H. Davis, J. Fluid Mech. **346**, 117 (1997).
[26] S. I. Ross, F. H. Verhoff, and R. I. Curl, Ind. Eng. Chem. Fundam. **17**, 101 (1978).
[27] M. A. Rother and R. H. Davis, Phys. Fluids **13**, 1178 (2001).
[28] L. G. Leal, Phys. Fluids **16**, 1833 (2004).
[29] N. Grizuti and O. Bifulco, Rheol. Acta **36**, 406 (1997).
[30] H. Mousa and T. G. M. van de Ven, Colloids Surf., A **95**, 221 (1995).
[31] R. McGraw, Aerosol Sci. Technol. **27**, 255 (1997).
[32] R. B. Diemer and J. H. Olson, Chem. Eng. Sci. **57**, 2211 (2002).
[33] M. J. Hounslow and X. Ni, Chem. Eng. Sci. **59**, 819 (2004).
[34] G. K. Batchelor and J. T. Green, J. Fluid Mech. **56**, 375 (1972).
[35] R. A. de Bruijn, Ph.D. thesis, Eindhoven University of Technology, Eindhoven, The Netherlands, 1989.
[36] G. Barnocky and R. H. Davis, Int. J. Multiphase Flow **15**, 627 (1989).
[37] M. Loewenberg and E. J. Hinch, J. Fluid Mech. **338**, 299 (1997).
[38] S. Guido and M. Villone, J. Colloid Interface Sci. **209**, 247 (1999).
[39] G. I. Taylor, Proc. R. Soc. London, Ser. A **146**, 501 (1934).
[40] A. J. Ramic, S. D. Hudson, A. M. Jamieson, and I. Manas-Zloczower, Polymer **41**, 6263 (2000).
[41] J. N. Israelachvili, J. Chem. Soc., Faraday Trans. 2 **69**, 1729 (1973).
[42] J. W. Jansen, C. G. de Kruif, and A. Vrij, J. Colloid Interface Sci. **114**, 471 (1986).
[43] M. A. Rother and R. H. Davis, J. Colloid Interface Sci. **214**, 297 (1999).
[44] S. Caserta, M. Simeone, and S. Guido, Rheol. Acta **43**, 491 (2004).
[45] G. Zhou and S. M. Kresta, Chem. Eng. Sci. **53**, 2099 (1998).